Research Article

Yanjun Sun, Jialu Wang, Beinan Jia, Long Chang, and Yongjun Jian*

Double diffusion convection of Maxwell–Cattaneo fluids in a vertical slot

https://doi.org/10.1515/phys-2024-0039
received January 17, 2024; accepted May 11, 2024

Abstract: The convection stability of Maxwell–Cattaneo fluids in a vertical double-diffusive layer is investigated. Maxwell–Cattaneo fluids mean that the response of the heat flux with respect to the temperature gradient satisfies a relaxation time law rather than the classical Fourier one. The Chebyshev collocation method is used to resolve the linearized forms of perturbation equations, leading to the formulation of stability eigenvalue problem. By numerically solving the eigenvalue problem, the neutral stability curves in the a–Gr plane for the different values of solute Rayleigh number $\mathrm{Ra_S}$ are obtained. Results show that increasing the double diffusion effect and Louis number Le can suppress the convective instability. Furthermore, compared with Fourier fluid, the Maxwell–Cattaneo fluids in a vertical slot cause an oscillation on the neutral stability curve. The appearance of Maxwell–Cattaneo effect enhances the convection instability. Meanwhile, it is interesting to find that the Maxwell–Cattaneo effect for convective instability becomes stronger as the Prandtl number rises. That means Prandtl number (Pr) also has a significant effect on convective instability. Moreover, the occurrence of two minima on the neutral curve can be found when Pr reaches 12.

Keywords: Maxwell–Cattaneo fluids, double diffusive convection, heat transfer, vertical slot

*** Corresponding author: Yongjun Jian,** Institute for Nonlinear Science, Donghua University, Shanghai, 201620, China; School of Mathematics and Statistics, Donghua University, Shanghai, 201620, China, e-mail: jianyj@dhu.edu.cn
Yanjun Sun: School of Mathematical Science, Inner Mongolia University, Hohhot, Inner Mongolia, 010021, China; School of Statistics and Mathematics, Inner Mongolia University of Finance and Economics, Hohhot, Inner Mongolia, 010070, China
Jialu Wang, Beinan Jia: School of Mathematical Science, Inner Mongolia University, Hohhot, Inner Mongolia, 010021, China
Long Chang: School of Statistics and Mathematics, Inner Mongolia University of Finance and Economics, Hohhot, Inner Mongolia, 010070, China

1 Introduction

Double-diffusive convection is a fluid flow phenomenon that arises from the interplay of buoyancy forces resulting from differences in diffusivity, propagation, and spatial distribution between two distinct constituents. This convection occurs when two components that contribute to density spread at different rates. In the past few decades, many researchers have drawn attention to the double diffusion convective flow induced by the buoyancy caused by the temperature and concentration gradients at the same time. This kind of flow is of great significance and has been widely used in oceanography [1,2], crystal growth [3–5], metal manufacturing process [6,7], ventilation [8–10], and other fields [11,12]. The first stability analysis to demonstrate the basic mechanism of double-diffusive was performed by Stern [13]. He found that a "gravitationally stable" stratification of salinity and temperature, such as is observed in the oceans, is unstable due to the fact that the molecular diffusivity of heat is much greater than the diffusivity of salt. This conclusion was expanded by Veronis [14] and Baines and Gill [15] a few years later. Some of the most recent contributions in this area include those of Shankar *et al.* [16] and Wang *et al.* [17].

It is widely acknowledged that the dynamical behavior exhibited by the double-diffusive fluid system is contingent upon both the magnitude and orientation of the initial gradients. Many scholars have focused on vertical double diffusion instability in recent years [18–22]. Among them, the double diffusion stability under the interaction of horizontal temperature gradient and concentration gradient has been studied extensively [23–27]. Ghorayeb and Mojtabi [28] studied the double diffusive convection in vertical enclosures with equal and opposing buoyancy forces due to horizontal thermal and concentration gradients. Makayssi *et al.* [29] investigated the natural double-diffusive convection for the Carreau shear-thinning fluid in a square cavity submitted to horizontal temperature and concentration gradients. The double-diffusive stability of the fluid in the vertical slot is featured with the Hopf bifurcation, when the concentration gradient is perpendicular

to the temperature gradient [30–34]. Zhang *et al.* [35] studied the effect of radiative heat transfer on thermal-solutal Marangoni convection in a shallow rectangular cavity with mutually perpendicular temperature and concentration gradients. Numerical simulation of thermal-solutal Marangoni convection in a shallow rectangular cavity with mutually perpendicular temperature and concentration gradients was investigated by Zhang *et al.* [36]. On the other hand, the Hopf bifurcation also happens when the temperature and concentration gradients are parallel in the horizontal direction. Huang and Chen [37] carried out the stability of the double-diffusive convection generated through the interaction of horizontal temperature and concentration gradients in the vertical slot.

In the above mentioned work, the heat transfer process in the form of diffusion is described by Fourier law [38]. It is well known that Fourier law produces a parabolic equation for the temperature field when coupled with the law of conservation of energy. The major drawback of heat conduction law is that it obeys the parabolic energy equation, which projected that a disturbance wave in the temperature field will move at an unlimited speed. Fourier's law of heat conduction is modified in a variety of ways and circumstances to avoid this characteristic [39–41]. These models extend the usual Fourier equation by including a new transient term. The new transient component is multiplied by a time constant, also known as the thermal relaxation time, which represents the time required for the heat flow to relax to a new steady state after a temperature gradient perturbation. In general, we refer to a fluid whose relaxation time is not negligible as a Maxwell–Cattaneo (or non-Fourier) fluid, and a fluid whose relaxation time is negligible as a Fourier one. Maxwell–Cattaneo fluids are used in a variety of applications, including low temperature liquids [42], nanofluids [43], convection in nano-devices [44], and fluids exposed to rapid heat transfer processes [45].

In the past few decades, many scholars have used analytical and numerical methods to study Maxwell–Cattaneo heat conduction under different conditions for solid materials [46–49]. For fluid flow and convection investigations, Stranges *et al.* [50] studied the finite thermal convection of Maxwell–Cattaneo fluids. They described the relationship between heat flux and temperature gradient changes and theoretically explored thermal convection in fluids with considerable thermal relaxation time. Hughes *et al.* [51] investigated the linear stability of a double-diffusive fluid layer and demonstrated that modifying Fick's law for either temperature or salinity can lead to the emergence of novel oscillation modes and significant alterations in the preferred wavelength of oscillatory convection at its onset. Thermal convection in a magnetized conducting fluid with the Cattaneo–Christov heat-flow model was studied by Bissell [52]. By replacing the conventional parabolic Fourier law with the Cattaneo–Christov heat-flow model, he investigated the influence of hyperbolic heat-flow effects on thermal convection in a magnetized conducting fluid layer heated from below. Hughes *et al.* [53] studied the linear stability of rotating convection, incorporating the Maxwell–Cattaneo effect. Eltayeb [54] investigated the linear and weakly nonlinear stabilities of a horizontal layer of fluid obeying the Maxwell–Cattaneo relationship of heat flux and temperature using three different forms of the time derivative of the heat flux, motivated by a desire to better understand the dynamics of Maxwell–Cattaneo fluids. At various temperatures, Niknami and Khayat [55] investigated the instability of steady natural convection between vertical surfaces of a single-phase hysteretic Maxwell–Cattaneo fluid. The linear stability analysis is performed for different Prandtl, Grashof, and Cattaneo numbers. The instability mechanism is discussed through an examination of the disturbance energy equation.

However, the available literature has not paid any attention to the stability of Maxwell–Cattaneo fluids in a vertical double-diffusive layer in which the boundaries are maintained at constant but differing temperatures and solute concentrations. In this study, we employ the normal mode method to analyze linear stability and assume that each disturbance can be decomposed into dynamically independent wave components. The objective of present work is to understand further the coupling phenomenon between non-Fourier fluids and double diffusion convection in a vertical slot.

2 Mathematical model

2.1 Governing equations

We consider a two-dimensional infinite vertical layer of a Newtonian Maxwell–Cattaneo liquid mixture subjected to a horizontal temperature and concentration gradients. The physical configuration is described by a Cartesian coordinate system (x^*, y^*) with the y^* axis in the vertical direction. The fluids are bounded by two parallel plates $x^* = -h^*/2$ and $x^* = h^*/2$ at which constant different temperatures T_L^* and $T_R^*(>T_L^*)$ as well as solute concentrations S_L^* and $S_R^*(>S_L^*)$, respectively as shown in Figure 1. The gravity acceleration vector is given by $\boldsymbol{g} = -g\boldsymbol{e_y}$, where $\boldsymbol{e_y}$ is the unit vector in the y^* direction. The fluid density ρ is assumed

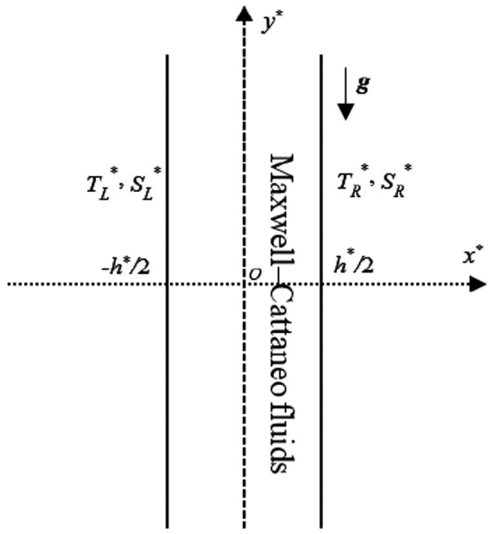

Figure 1: Schematic of the physical configuration.

to vary linearly with temperature T^* and solute concentration S^* in the form

$$\rho = \rho_0[1 - \alpha_T(T^* - T_0) + \alpha_S(S^* - S_0)], \tag{1}$$

where ρ_0 is the reference density at reference temperature $T_0 = (T_R^* + T_L^*)/2$ and reference solute concentration $S_0 = (S_R^* + S_L^*)/2$, α_T is the volumetric thermal expansion coefficient, and α_S is the solute analog of α_T. The fluid is assumed to be incompressible, with specific heat at constant pressure c_p, thermal conductivity k, and mass diffusivity D. The fluid behavior is described by equations for the conservation of mass, linear momentum, energy, and concentration. In this case, with the usual Boussinesq's approximation, the governing equations can be expressed as follows:

$$\nabla^* \cdot \boldsymbol{u}^* = 0, \tag{2}$$

$$\rho_0(\boldsymbol{u}_{t^*}^* + \boldsymbol{u}^* \cdot \nabla^* \boldsymbol{u}^*) = -\nabla^* p^* - \rho g \boldsymbol{e}_y + \mu \nabla^{*2} \boldsymbol{u}^*, \tag{3}$$

$$\rho_0 c_p(T_{t^*}^* + \boldsymbol{u}^* \cdot \nabla^* T^*) = -\nabla^* \cdot \boldsymbol{Q}^*, \tag{4}$$

$$S_{t^*}^* + \boldsymbol{u}^* \cdot \nabla^* S^* = D \nabla^{*2} S^*, \tag{5}$$

where $\boldsymbol{u}^* = (u^*, v^*)$ is the velocity vector, t^* is the time, p^* is the pressure, μ is the dynamic viscosity of the fluid, T^* is the temperature, S^* is the concentration, and $\boldsymbol{Q}^*$ is the heat flux vector. For Maxwell–Cattaneo fluids, the heat flux is assumed to be governed by [39]

$$\tau \frac{\delta \boldsymbol{Q}^*}{\delta t^*} + \boldsymbol{Q}^* = -k \nabla^* T^*. \tag{6}$$

Here we adopt the formulation of Christov [41], who proposed the frame-invariant equation for the development of the heat flux as follows:

$$\frac{\delta \boldsymbol{Q}^*}{\delta t^*} = \frac{\partial \boldsymbol{Q}^*}{\partial t^*} + \boldsymbol{u}^* \cdot \nabla^* \boldsymbol{Q}^* - \boldsymbol{Q}^* \cdot \nabla^* \boldsymbol{u}^* + \boldsymbol{Q}^* \nabla^* \cdot \boldsymbol{u}^*, \tag{7}$$

τ is the thermal relaxation time of the medium and characterizes the relaxation of the heat flux to a new steady state following a perturbation of the temperature field. The introduction of a finite relaxation time changes the fundamental nature of the parabolic heat equation of Fourier fluids, in which heat diffuses with infinite speed, to a hyperbolic heat equation with a solution in the form of a heat wave that propagates with finite speed. This change in the Maxwell–Cattaneo fluid will eventually exhibit a disturbance that is completely different from that of the Fourier fluid. The boundary conditions at the wall are expressed as follows:

$$u^* = 0, \quad v^* = 0, \quad T^* = T_L, \quad S^* = S_L, \quad \text{at} \quad x^* = -\frac{h}{2}, \tag{8}$$

$$u^* = 0, \quad v^* = 0, \quad T^* = T_R, \quad S^* = S_R, \quad \text{at} \quad x^* = \frac{h}{2}. \tag{9}$$

We use the following set of scales to nondimensionalize the above governing system:

$$\begin{aligned} &x = \frac{x^*}{h}, \quad y = \frac{y^*}{h}, \quad \boldsymbol{u} = \frac{\boldsymbol{u}^*}{\rho_0 g \alpha_T (T_R - T_L) h^2/\mu}, \\ &p = \frac{p^* + \rho_0 g}{\rho_0 g \alpha_T (T_R - T_L) h}, \\ &t = \frac{t^*}{\rho_0 h^2/\mu}, \quad \theta = \frac{T^* - T_0}{T_R - T_L}, \quad S = \frac{S^* - S_0}{S_R - S_L}, \\ &\boldsymbol{Q} = \frac{\boldsymbol{Q}^*}{k(T_R - T_L)/h}. \end{aligned} \tag{10}$$

Using the dimensionless variables above, the governing equations reduce to the following forms:

$$\nabla \cdot \boldsymbol{u} = 0, \tag{11}$$

$$\boldsymbol{u}_t + \mathrm{Gr} \boldsymbol{u} \cdot \nabla \boldsymbol{u} = -\nabla p + \nabla^2 \boldsymbol{u} + \left(\theta - \frac{\mathrm{Ra_S}}{\mathrm{GrPr}} S\right) \boldsymbol{e}_y, \tag{12}$$

$$\frac{1}{\mathrm{Gr}} S_t + \boldsymbol{u} \cdot \nabla S = \frac{1}{\mathrm{GrPrLe}} \nabla^2 S, \tag{13}$$

$$\theta_t + \mathrm{Gr} \boldsymbol{u} \cdot \nabla \theta = -\frac{1}{\mathrm{Pr}} \nabla \cdot \boldsymbol{Q}. \tag{14}$$

The governing equation of the heat flux can be obtained from Eqs. (6) and (7) as

$$C\mathrm{Pr} \boldsymbol{Q}_t + C\mathrm{PrGr}(\boldsymbol{u} \cdot \nabla \boldsymbol{Q} - \boldsymbol{Q} \cdot \nabla \boldsymbol{u}) + \boldsymbol{Q} = -\nabla \theta. \tag{15}$$

In the above equations, the following non-dimensional parameters are defined:

$$\begin{aligned} \mathrm{Gr} &= \frac{g\alpha_T(T_R - T_L)h^3}{\nu^2}, \quad \mathrm{Pr} = \frac{\nu}{\kappa}, \quad C = \frac{\tau\kappa}{h^2}, \\ \mathrm{Ra_S} &= \frac{\alpha_S g(S_R - S_L)h^3}{\nu\kappa}, \quad \mathrm{Le} = \frac{\kappa}{D}. \end{aligned} \tag{16}$$

where $\kappa = k/(\rho_0 c_p)$ is the thermal diffusivity, $\nu = \mu/\rho_0$ is the kinematic viscosity, Gr is the Grashof number, Pr is the Prandtl number, C is the Cattaneo number, $\mathrm{Ra_S}$ is the solute Rayleigh number, and Le is the Lewis number. The Maxwell–Cattaneo effect in heat transfer is mainly described by the Cattaneo number, which is defined by the ratio of the thermal relaxation time to the thermal diffusion time [45]. The dimensionless boundary conditions are

$$u = 0, \quad v = 0, \quad \theta = \pm\frac{1}{2}, \quad S = \pm\frac{1}{2}, \quad \text{at} \quad x = \pm\frac{1}{2}. \tag{17}$$

2.2 Basic solution

The basic state is assumed that the motion is stable and independent of the vertical coordinates. In this case, the base solutions can be expressed as

$$\begin{aligned} &u = \bar{u}(x), \quad v = \bar{v}(x), \quad p = \bar{p}(x), \quad \theta = \bar{\theta}(x), \\ &S = \bar{S}(x), \quad q_x = \bar{q}_x(x), \quad q_y = \bar{q}_y(x), \end{aligned} \tag{18}$$

where q_x and q_y are the dimensionless heat flux components in the x and y directions, respectively. Then, the basic solutions can be obtained from Eqs. (11)–(15), combined with Eq. (17) as follows:

$$\bar{u} = 0, \quad \bar{v} = -\frac{1}{6}\left(1 - \frac{\mathrm{Ra_S}}{\mathrm{GrPr}}\right)x^3 + \frac{1}{24}\left(1 - \frac{\mathrm{Ra_S}}{\mathrm{GrPr}}\right)x, \tag{19a}$$

$$\bar{\theta} = x, \quad \bar{S} = x,$$

$$\bar{q}_x = -1, \quad \bar{q}_y = \frac{1}{24}C\mathrm{PrGr}\left(1 - \frac{\mathrm{Ra_S}}{\mathrm{GrPr}}\right)(12x^2 - 1). \tag{19b}$$

If we set $\mathrm{Ra_S} = 0$, the base solution of Eq. (19a) can be reduced to the results obtained by Niknami and Khayat [55]. To accomplish meaningful and thoughtful theoretical research, we carry out the stability analysis with wide ranges of Pr and C for the Maxwell–Cattaneo fluid. A wide range of values for the Prandtl number Pr is chosen from 0.7 to 15, and the Cattaneo number C is chosen from 10^{-3} to 10^{-2} in this study [18,51]. Interestingly, Eq. (19b) shows that the heat flux in the y direction is proportional to the Cattaneo number, indicating that Maxwell–Cattaneo effects play a significant role in basic solutions. Clearly, for a Fourier fluid ($C = 0$), q_y becomes zero. The appearance of non-Fourier effect term in the basic solution will change the stability of the basic flow.

Figure 2(a) illustrates the base velocity in the y-direction with different $\mathrm{Ra_S}$ when Gr = 1000, Le = 1, and Pr = 1. It demonstrates that the base flow is reduced with the increase in the double diffusion effect $\mathrm{Ra_S}$. Also, for the prescribed $\mathrm{Ra_S}$, a single closed cell of fluid is structured by descending along the cold wall and rising along the hot wall. In Figure 2(b), the heat flux in the y-direction is shown for variational values of Cattaneo number C, as Gr = 1000, Pr = 1, Le = 1, and $\mathrm{Ra_S} = 50$. As the Cattaneo number increases,

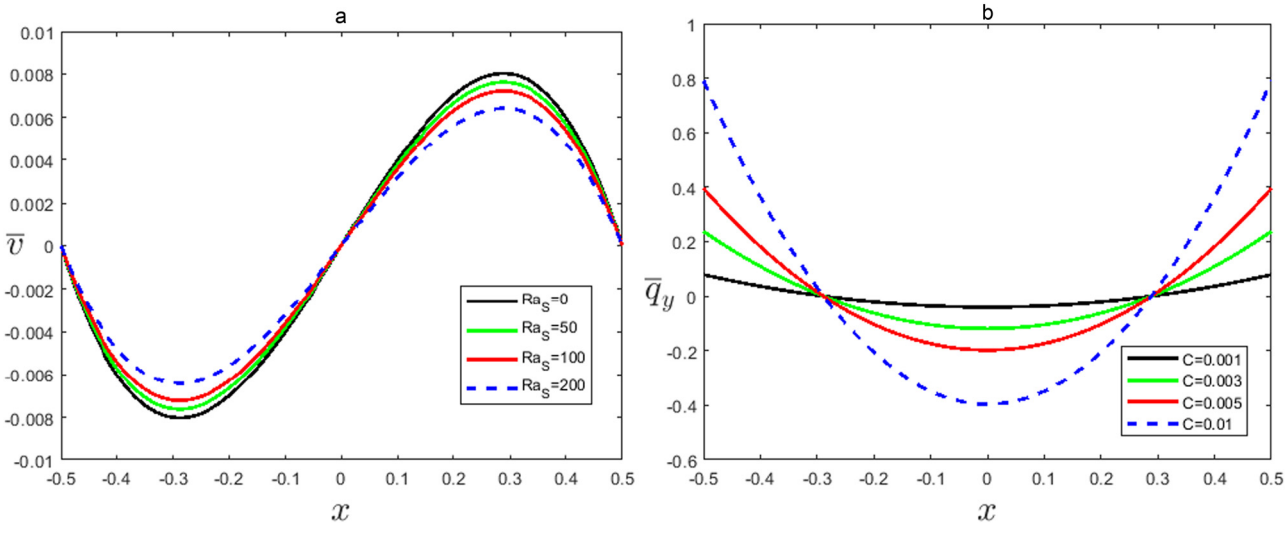

Figure 2: (a) The base flow velocity in the y-direction with different $\mathrm{Ra_S}$, when Gr = 1000, Pr = 1, and Le = 1. (b) The heat flux in the y-direction with different C, when Gr = 1000, Pr = 1, Le = 1, and $\mathrm{Ra_S} = 50$.

the magnitude for the heat flux in the y-direction increases when the double diffusion effect is taken into account.

3 Linear stability analysis

We now superimpose the small-amplitude disturbances on the basic state and study the stability of the system. By rewriting the constitutive equation for heat flux in terms of the scalar variable $F = \nabla\cdot\boldsymbol{Q}$, the problem can be made simpler. Taking the divergence of Eq. (15), and using the identity $\nabla\cdot(\mathbf{a}\cdot\nabla\mathbf{b}) = \nabla\mathbf{a}:\nabla\mathbf{b} + \mathbf{a}\cdot\nabla(\nabla\mathbf{b})$, we can obtain the following constitutive equation for F:

$$C\mathrm{Pr}F_t + C\mathrm{PrGr}\boldsymbol{u}\cdot\nabla F + F = -\nabla^2\theta. \tag{20}$$

Thus, Eq. (14) can be rewritten as

$$\theta_t + \mathrm{Gr}\boldsymbol{u}\cdot\nabla\theta = -\frac{1}{\mathrm{Pr}}F. \tag{21}$$

Using infinitesimal disturbances on the fully developed laminar base flow, the solution of the problem can be written in the form

$$\begin{aligned} u &= \bar{u} + u', \quad v = \bar{v} + v', \quad p = \bar{p} + p', \\ \theta &= \bar{\theta} + \theta', \quad F = \bar{F} + F', \quad S = \bar{S} + S', \end{aligned} \tag{22}$$

where the prime indicates that the quantities are infinitesimal perturbations. Substituting the above expressions of (22) into Eqs. (11)–(13), (20), and (21), and considering the first order disturbances, the following equations are obtained:

$$\frac{\partial u'}{\partial x} + \frac{\partial v'}{\partial y} = 0, \tag{23}$$

$$\frac{\partial u'}{\partial t} + \mathrm{Gr}\bar{v}\frac{\partial u'}{\partial y} = -\frac{\partial p'}{\partial x} + \left(\frac{\partial^2 u'}{\partial x^2} + \frac{\partial^2 u'}{\partial y^2}\right), \tag{24}$$

$$\begin{aligned} \frac{\partial v'}{\partial t} + \mathrm{Gr}\left(\frac{\mathrm{d}\bar{v}}{\mathrm{d}x}u' + \bar{v}\frac{\partial v'}{\partial y}\right) &= -\frac{\partial p'}{\partial y} + \left(\frac{\partial^2 v'}{\partial x^2} + \frac{\partial^2 v'}{\partial y^2}\right) \\ &\quad + \theta' - \frac{\mathrm{Ra_S}}{\mathrm{GrPr}}S', \end{aligned} \tag{25}$$

$$\mathrm{Pr}\frac{\partial\theta'}{\partial t} + \mathrm{PrGr}\left(\frac{\mathrm{d}\bar{\theta}}{\mathrm{d}x}u' + \bar{v}\frac{\partial\theta'}{\partial y}\right) = -F', \tag{26}$$

$$C\mathrm{Pr}\frac{\partial F'}{\partial t} + C\mathrm{PrGr}\bar{v}\frac{\partial F'}{\partial y} = -F' - \frac{\partial^2\theta'}{\partial x^2} - \frac{\partial^2\theta'}{\partial y^2}, \tag{27}$$

$$\frac{1}{\mathrm{Gr}}\frac{\partial S'}{\partial t} + u'\frac{\partial\bar{S}}{\partial x} + \bar{v}\frac{\partial S'}{\partial y} = \frac{1}{\mathrm{GrPrLe}}\left(\frac{\partial^2 S'}{\partial x^2} + \frac{\partial^2 S'}{\partial y^2}\right). \tag{28}$$

The corresponding disturbed boundary conditions are

$$u'\left(\pm\frac{1}{2}\right) = 0, \quad v'\left(\pm\frac{1}{2}\right) = 0, \quad \theta'\left(\pm\frac{1}{2}\right) = 0, \quad S'\left(\pm\frac{1}{2}\right) = 0. \tag{29}$$

We assume that the perturbation variables take the form

$$\{u', v', p', \theta', S', F'\} = \{U, V, \Pi, \Theta, \Phi, f\}(x)e^{st+iay}, \tag{30}$$

where s dictates the time evolution of the disturbance and a is the real wave number. Substituting Eq. (30) in Eqs. (23)–(28), we get

$$\frac{\mathrm{d}U}{\mathrm{d}x} + iaV = 0, \tag{31}$$

$$(s + ia\bar{v}\mathrm{Gr})U = -\frac{\mathrm{d}\Pi}{\mathrm{d}x} + \frac{\mathrm{d}^2U}{\mathrm{d}x^2} - a^2U, \tag{32}$$

$$\begin{aligned} (s + ia\bar{v}\mathrm{Gr})V + \mathrm{Gr}\frac{\mathrm{d}\bar{v}}{\mathrm{d}x}U &= -ia\Pi + \frac{\mathrm{d}^2V}{\mathrm{d}x^2} - a^2V + \Theta \\ &\quad - \frac{\mathrm{Ra_S}}{\mathrm{PrGr}}\Phi, \end{aligned} \tag{33}$$

$$s\mathrm{Pr}\Theta + \mathrm{PrGr}\left(\frac{\mathrm{d}\bar{\theta}}{\mathrm{d}x}U + ia\bar{v}\Theta\right) = -f, \tag{34}$$

$$(sC\mathrm{Pr} + iaC\mathrm{PrGr}\bar{v} + 1)f = -\frac{\mathrm{d}^2\Theta}{\mathrm{d}x^2} + a^2\Theta, \tag{35}$$

$$s\frac{1}{\mathrm{Gr}}\Phi + \frac{\partial\bar{S}}{\partial x}U + ia\bar{v}\Phi = \frac{1}{\mathrm{GrPrLe}}\left(\frac{\mathrm{d}^2\Phi}{\mathrm{d}x^2} - a^2\Phi\right). \tag{36}$$

Since the problem is two-dimensional, the stream function formulation $\psi(x, y, t) = \Psi(x)e^{st+iay}$ is introduced such that the continuity equation is satisfied

$$U = ia\Psi, \quad V = -\frac{\mathrm{d}\Psi}{\mathrm{d}x}. \tag{37}$$

By substituting Eq. (37) in Eqs. (31)–(36), and eliminating $\Pi(x)$ and $f(x)$, we obtain the ordinary differential eigenvalue problem

$$\begin{aligned} \frac{\mathrm{d}^4\Psi}{\mathrm{d}x^4} &= (2a^2 + s + ia\mathrm{Gr}\bar{v})\frac{\mathrm{d}^2\Psi}{\mathrm{d}x^2} - \left(a^4 + a^2s + ia^3\mathrm{Gr}\bar{v}\right. \\ &\quad \left. + ia\mathrm{Gr}\frac{\mathrm{d}^2\bar{v}}{\mathrm{d}x^2}\right)\Psi + \frac{\mathrm{d}\Theta}{\mathrm{d}x} - \frac{\mathrm{Ra_S}}{\mathrm{GrPr}}\frac{\mathrm{d}\Phi}{\mathrm{d}x}, \end{aligned} \tag{38}$$

$$\frac{\mathrm{d}^2\Theta}{\mathrm{d}x^2} = ia\mathrm{PrGr}\Lambda\frac{\mathrm{d}\bar{\theta}}{\mathrm{d}x}\Psi + (s\mathrm{Pr}\Lambda + ia\mathrm{PrGr}\Lambda\bar{v} + a^2)\Theta, \tag{39}$$

$$\begin{aligned} \frac{\mathrm{d}^2\Phi}{\mathrm{d}x^2} &= ia\mathrm{GrPrLe}\frac{\mathrm{d}\bar{S}}{\mathrm{d}x}\Psi + (\mathrm{PrLe}s + ia\mathrm{GrPrLe}\bar{v} \\ &\quad + a^2)\Phi, \end{aligned} \tag{40}$$

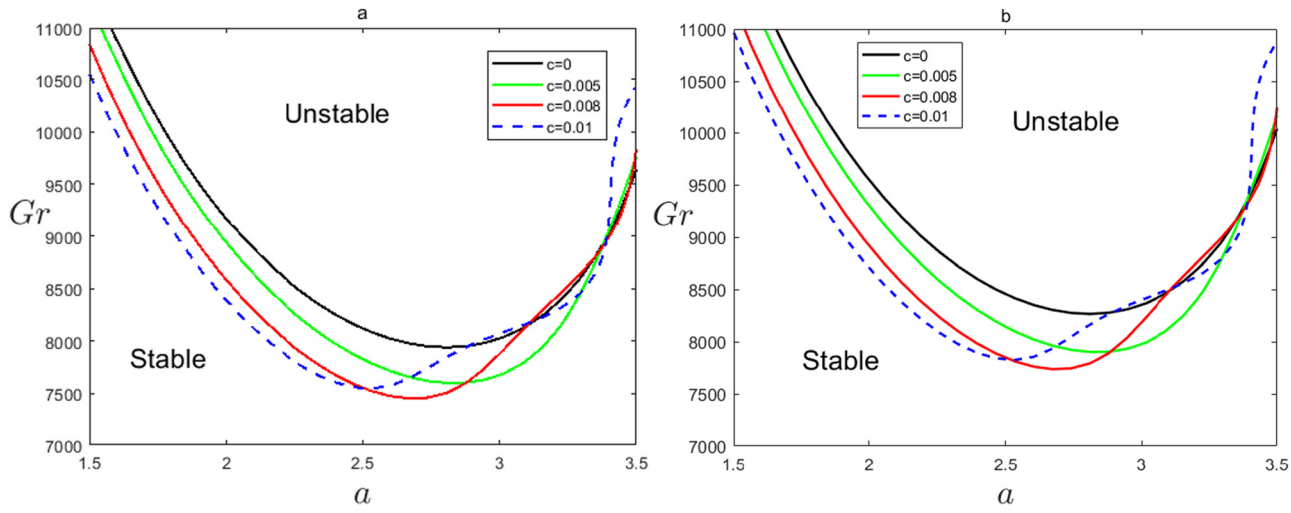

Figure 3: The neutral curve in the a–Gr plane with the different values of C. (a) Pr = 1 and Ra_S = 0. (b) Le = 1, Pr = 1, and Ra_S = 200.

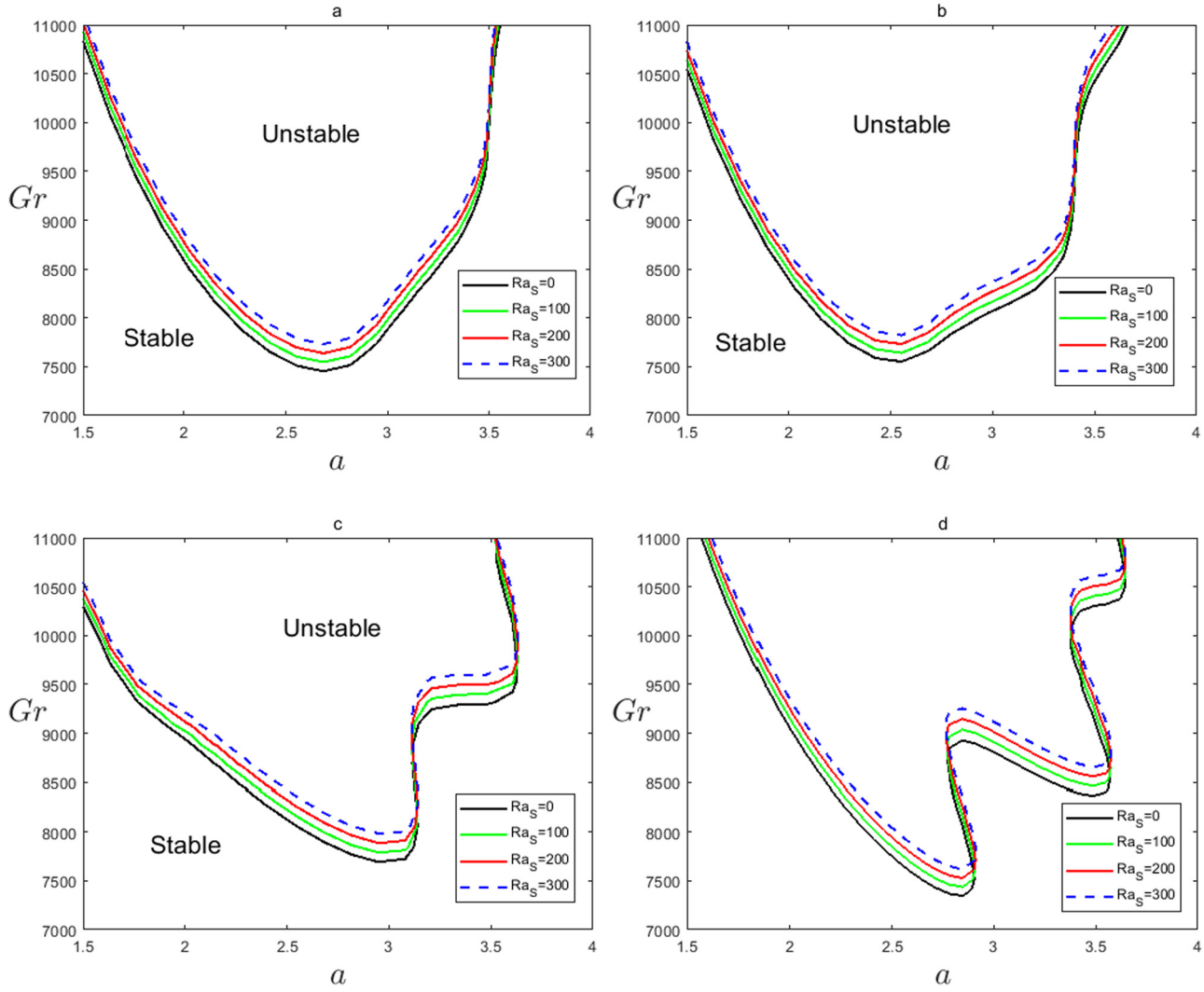

Figure 4: The neutral curve in the a–Gr plane for diverse values of Ra_S when Le = 1 and Pr = 1. (a) C = 0.008, (b) C = 0.01, (c) C = 0.015, and (d) C = 0.02.

where $\Lambda = sC\mathrm{Pr} + iaC\mathrm{Pr}\mathrm{Gr}\bar{v} + 1$. The relevant boundary conditions are

$$\Psi = \frac{\partial \Psi}{\partial x} = 0, \quad \Theta = 0, \quad \Phi = 0, \quad \text{at} \quad x = \pm\frac{1}{2}. \tag{41}$$

4 Result and discussion

Linear stability analysis and numerical simulation of Maxwell–Cattaneo fluids with double diffusion convective in a vertical slab is carried out. We use the Chebyshev collocation method to resolve the linearized forms of perturbation equations. The Chebyshev polynomial of nth order is given by

$$\xi_n(x) = \cos(n\cos^{-1}x), \quad x_j = \cos\left(\frac{\pi j}{N}\right), \quad j = 0, 1, \ldots, N, \tag{42}$$

where x_j are the Chebyshev collocation points and N is any positive integer. The Chebyshev polynomials are used to approximate the field variables

$$\begin{aligned} \Psi(x) &= \sum_{n=0}^{N} \Psi_n \xi_n(x), \\ \Theta(x) &= \sum_{n=0}^{N} \Theta_n \xi_n(x), \\ \Phi(x) &= \sum_{n=0}^{N} \Phi_n \xi_n(x). \end{aligned} \tag{43}$$

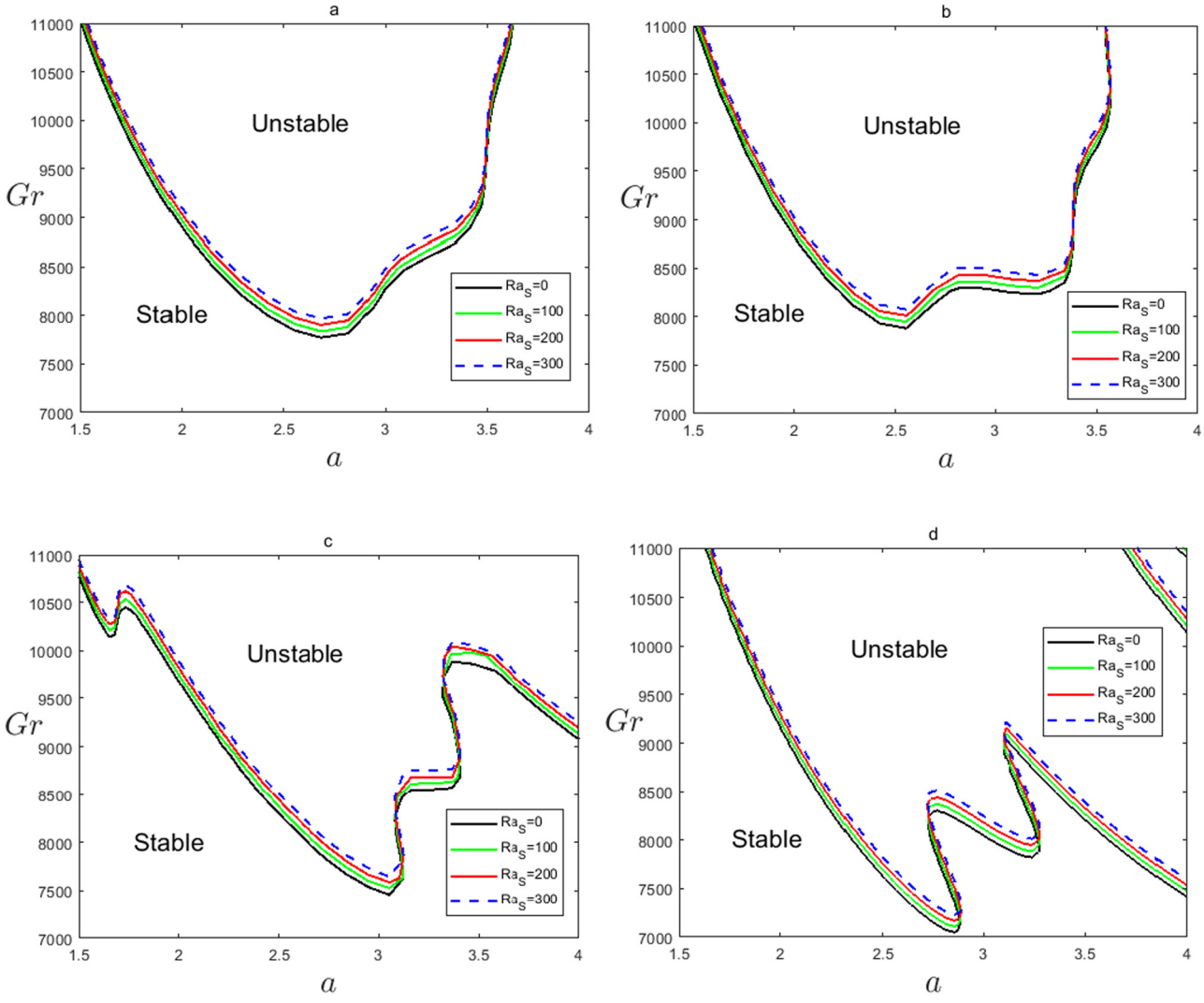

Figure 5: The neutral curve in the a–Gr plane with diverse values of $\mathrm{Ra_S}$ when Le = 1 and Pr = 1.5. (a) C = 0.008, (b) C = 0.01, (c) C = 0.015, and (d) C = 0.02.

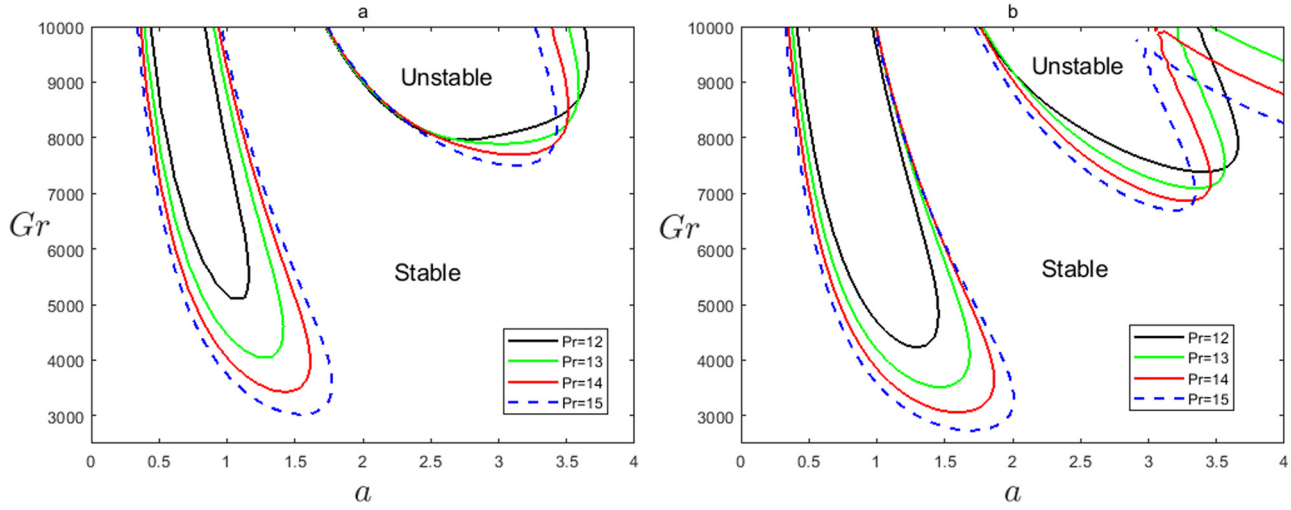

Figure 6: The neutral curve in the a–Gr plane for diverse values of Pr when Le = 0.5 and Ra_S = 50. (a) C = 0.001 and (b) C = 0.0015.

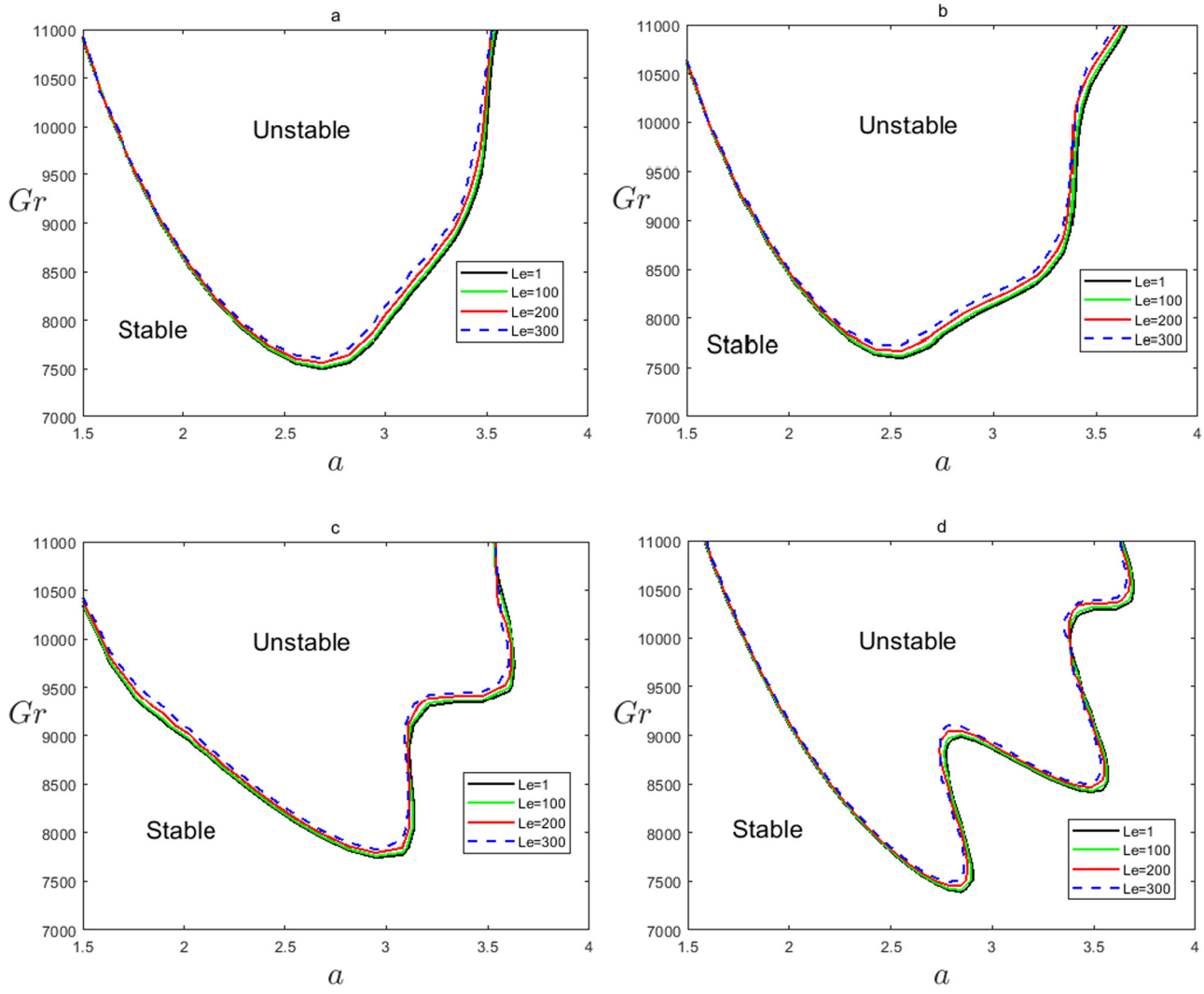

Figure 7: The neutral curve in the a–Gr plane for diverse values of Le when Ra_S = 50 and Pr = 1. (a) C = 0.008, (b) C = 0.01, (c) C = 0.015, and (d) C = 0.02.

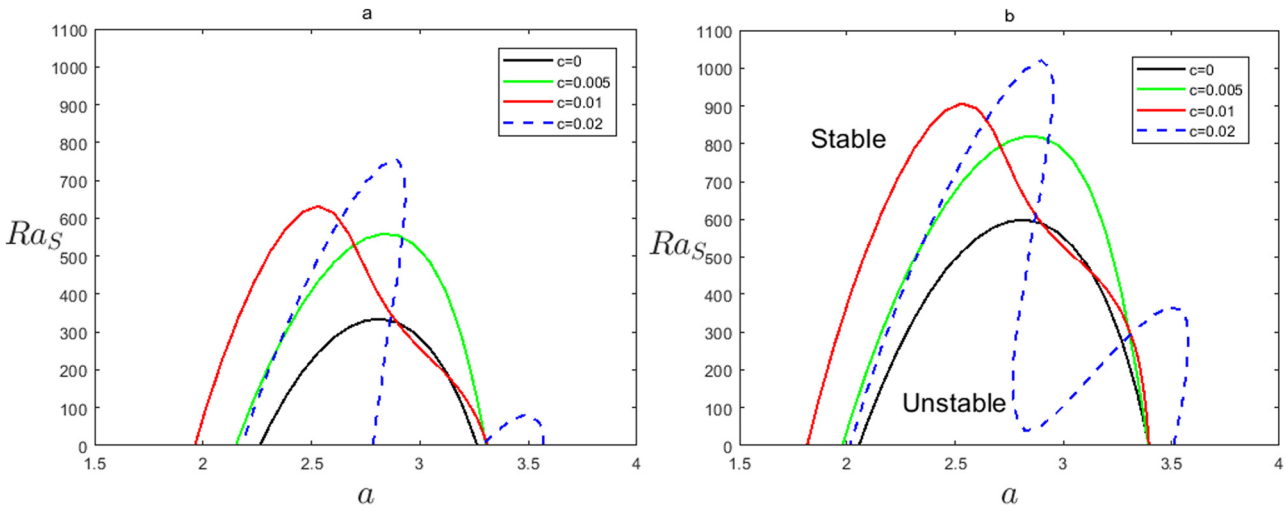

Figure 8: The neutral curve in the a–$\mathrm{Ra_S}$ plane for different values of C when Le = 1 and Pr = 1. (a) Gr = 8500 and (b) Gr = 9000.

The Eqs. (38)–(40) can be discretized and lead to a generalized eigenvalue problem of the form

$$\boldsymbol{A}_0 X + s\boldsymbol{A}_1 \boldsymbol{X} + s^2 \boldsymbol{A}_2 \boldsymbol{X} = \boldsymbol{0}, \tag{44}$$

where s and $\boldsymbol{X}$ are the complex eigenvalue and eigenfunction, respectively, and $\boldsymbol{A}_0$, $\boldsymbol{A}_1$, and $\boldsymbol{A}_2$ are square complex matrices of rank $2N + 2$. The eigenvalues are computed numerically by using the MATLAB routine polyeig.

We choose the parameter values given by Niknami and Khayat [55] to validate the numerical code. The neutral curve in the a–Gr plane is presented in Figure 3(a) when $\mathrm{Ra_S} = 0$, with the value of C varying between 0 and 0.01. It shows an excellent agreement between the current result and the result of Niknami and Khayat [55]. Neutral stability curves in the a–Gr plane with the different values of C, when Le = 1, Pr = 1, and $\mathrm{Ra_S} = 200$, are depicted in Figure 3(b). This figure illustrates the unstable domain decreases with the increase in the value of $\mathrm{Ra_S}$ compared with the results in Figure 3(a). Therefore, the increasing value of $\mathrm{Ra_S}$ has a stabilizing effect. In addition, the stable region becomes oscillation when the relaxation time is increasing if the double diffusion effect is taken into account.

Figures 4 and 5, respectively, show images of neutral stability curves in the a–Gr plane for different $\mathrm{Ra_S}$ values, where Pr = 1 and Pr = 1.5 are used to study the impact of the double diffusion effect when Cattaneo number C = 0.008, 0.01, 0.015, and 0.02, respectively. From Figure 4, the unstable regions shrink as the $\mathrm{Ra_S}$ increases, indicating that the double diffusion effect compresses convective instability. In Figure 4a, there is also a little amount of jitter

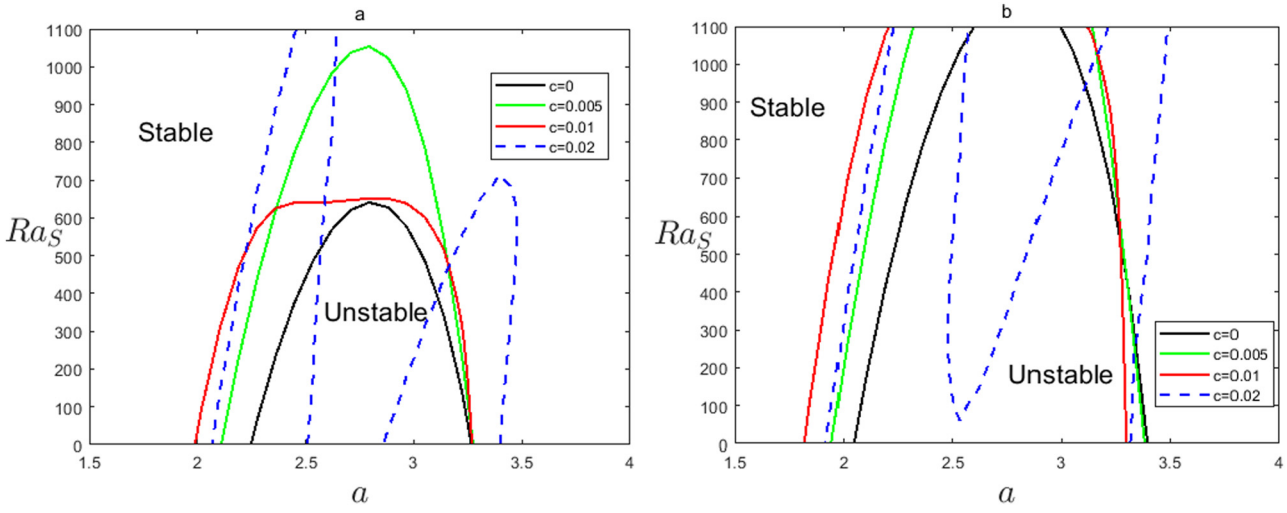

Figure 9: The neutral curve in the a–$\mathrm{Ra_S}$ plane for different values of C when Le = 1 and Pr = 1.1. (a) Gr = 8500 and (b) Gr = 9000.

in the neutral stability curve caused by the non-zero Cattaneo number C. Comparing Figure 4a–d, it can be seen that the jitter of the neutral stability curve increases with the Cattaneo number C for a prescribed Ra_S. This result is consistent with the one given by Niknami and Khayat [55]. In addition, by comparing Figures 4 and 5, it can be seen that the oscillation of the neutral stability curve increases as Pr increases. However, the inhibitory effect of double diffusion on instability remains unchanged. Moreover, Figure 5 demonstrates that the instability regions significantly increase with the increase in the values of Cattaneo number C when Pr = 1.5. This implies that the Maxwell–Cattaneo effect for the convective instability is enhanced as the Prandtl number increases.

Figure 6 shows the images of neutral stability curves in the a–Gr plane for different Pr values, where Le = 1 and Ra_S = 50 are used to study the impact of the Prandtl number when Cattaneo number C = 0.001 and 0.0015, respectively. For Pr = 1, Figure 4, the neutral curve is an open single branch curve. As Pr increases to 12, Figure 6, the neutral curve is composed of two branches, the oscillating convective branch and the stationary branch. In this case, the neutral curve changed from the travelling-wave mode to the stationary mode with the increase in the wave number. This result is consistent with prior findings by other researchers [18,37]. On the other hand, the unstable stability curve appears to contain two minimums, indicating that the mode of instability has regions expanding as the Pr increases, indicating that the Prandtl number enhances the convective instability.

Figure 7 illustrate the images of neutral stability curves in the a–Gr plane for different Le values, where Ra_S = 50 and Pr = 1 are used to study the impact of the Lewis number effect when the Cattaneo number C = 0.008, 0.01, 0.015, and 0.02,

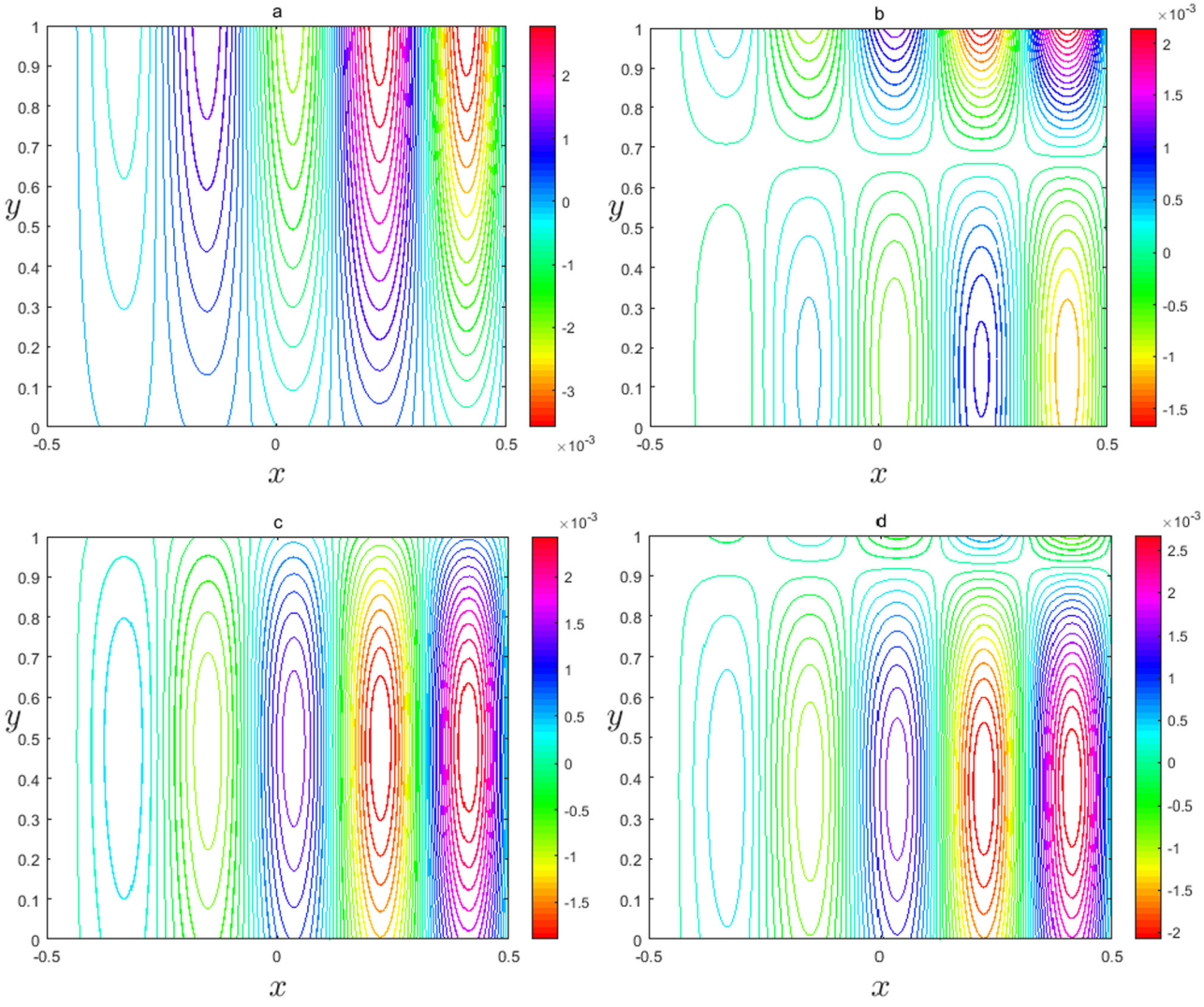

Figure 10: Disturbance streamlines when Gr = 11000, a = 1.5, Le = 1, Pr = 1, and Ra_S = 100. (a) C = 0.005, (b) C = 0.008, (c) C = 0.01, and (d) C = 0.02.

respectively. The Lewis number is the ratio of thermal and mass diffusivity. Therefore, Le increases with the increase in thermal diffusivity or decrease in mass diffusivity. From Figure 7, we observe that the unstable regions will gradually decrease with the increase in Le. The physical interpretation is that the Lewis number decreases the rate of heat and mass transfer, and as a result, the system becomes stable. This means that the Lewis number effect compresses convective instability. This result reported by Jakhar and Kumar [56] are reproduced with very good agreement. On the other hand, comparing Figure 7a–d, it is found that with the increase in C, the influence of Le on convective instability becomes smaller and smaller. It is demonstrated that the Maxwell–Cattaneo effect, compared with the Le effect, plays a dominant role in the instability of the system.

The distribution of the neutral stability curve in the a-Ra_S plane when the Cattaneo number C = 0, 0.005, 0.01, and 0.02, respectively, is depicted in Figures 8 and 9. The shrinking of the unstable regime is demonstrated in Figure 8a as the double diffusion effect intensifies. Moreover, under constant values of all other parameters, the flow will exhibit stability once Ra_S reaches a maximum. This finding provides further support for the stabilizing effects of double diffusion. When the Gr number drops from 9000 to 8500, comparing Figure 8a and b, it can be found that the unstable zone is greatly diminished and the inhibitory effect of the double diffusion effect becomes more evident as the Gr number lowers. Both of the aforementioned figures demonstrate that as relaxation time increases, there is also an increase in the oscillation of the parameter's marginal stability value. Comparing Figures 8 and 9, it can be found that the instability regions increase with the value of Pr.

Figure 10 gives the streamline pattern for different values of C with critical values of Gr when a = 1.5, Le = 1, Pr = 1, and Ra_S = 100. With C taking large values, the streamlines are seen more toward the boundary with higher temperature. That means the velocity of disturbance flowing in heat side is bigger than that in the cool side.

5 Conclusion

In this study, the convection stability problem of Maxwell–Cattaneo fluids in a vertical double-diffusive layer is investigated. The perturbation equations can be obtained by combining the incompressible Navier–Stokes equations of Maxwell–Cattaneo fluid with the boundary conditions. Furthermore, the Chebyshev collocation method is utilized to resolve the linearized forms of perturbation equations, resulting in the formulation of the stability eigenvalue problem. The results are summarized as follows:

- The instability is inhibited by both the double diffusion effect and the Lewis number.
- The neutral stability curve of Maxwell–Cattaneo fluid is found to oscillate, which differs from the Fourier fluid. Furthermore, the oscillation increases further with an increase in the Cattaneo number C.
- The Maxwell–Cattaneo effect has a greater impact on convective instability as the Prandtl number increases.
- The presence of the Maxwell–Cattaneo effect weakens the instability caused by the Lewis number in the system.
- The neutral curve of Maxwell–Cattaneo fluid exhibits oscillating convective branches and stationary branches, with two minima at a smaller Pr number (Pr = 12) compared to the Fourier fluid.

Funding information: This work was supported by the National Natural Science Foundation of China (Grant No. 12262026), the Natural Science Foundation of Inner Mongolia Autonomous Region of China (Grant No. 2021MS01007), the Research Program of Science and Technology at Universities of Inner Mongolia Autonomous Region (Grant No. NJZY23054), the Program for Innovative Research Team in Universities of Inner Mongolia Autonomous Region (Grant No. NMGIRT2323), the Inner Mongolia Grassland Talent (Grant No. 12000-12102013), the Fundamental Research Funds for the Central Universities (Grant Nos 2232022G-13, 2232023G-13, and 2232024G-13), and the Research Program of Basic Research Funds for Universities Directly Under the Inner Mongolia Autonomous Region (Grant No. NCYWT23035).

Author contributions: All authors have accepted responsibility for the entire content of this manuscript and approved its submission.

Conflict of interest: The authors state no conflict of interest.

References

[1] Schmidt RW. Double diffusion in oceanography. Annu Rev Fluid Mech. 1994;26(1):255–85.
[2] Carpenter JR, Sommer T, Wüest A. Stability of a double-diffusive interface in the diffusive convection regime. J Phys Oceanogr. 2012;42(5):840–54.
[3] Huppert HE, Sparks RSJ. Double diffusive convection due to crystallization in magmas. Annu Rev Earth Planet Sci. 1984;12(1):11–37.
[4] Zhou H, Zebib A. Oscillatory double-diffusive convection in crystal growth. J Cryst Growth. 1994;135(3–4):587–93.

[5] Chamkha AJ, Al-Naser H. Hydromagnetic double-diffusive convection in a rectangular enclosure with opposing temperature and concentration gradients. Int J Heat Mass Transf. 2002;45(12):2465–83.
[6] Nield DA, Kuznetsov AV. The onset of double-diffusive convection in a nanofluid layer. Int J Heat Fluid Flow. 2011;32(4):771–6.
[7] Kim J, Kang YT, Choi CK. Soret and Dufour effects on convective instabilities in binary nanofluids for absorption application. Int J Refrig. 2007;30(2):323–8.
[8] Geng J, Nie C, Marlow WH. Polydisperse aerosol condensation with heat and mass conservation: I. Model description with applications to homogeneous systems. Int J Heat Mass Transf. 2012;55(9–10):2429–39.
[9] Serrano-Arellano J, Xamán J, Álvarez G. Optimum ventilation based on the ventilation effectiveness for temperature and CO_2 distribution in ventilated cavities. Int J Heat Mass Transf. 2013;62:9–21.
[10] Malashetty MS, Gaikwad SN, Swamy M. An analytical study of linear and non-linear double diffusive convection with Soret effect in couple stress liquids. Int J Therm Sci. 2006;45(9):897–907.
[11] Naveen Kumar SB, Shivakumara IS, Shankar BM. Linear and weakly nonlinear double-diffusive magnetoconvection in a non-Newtonian fluid layer. Microgravity Sci Tec. 2020;32:629–46.
[12] Wang L, Shi B, Chai Z, Yang X. Regularized lattice Boltzmann model for double-diffusive convection in vertical enclosures with heating and salting from below. Appl Therm Eng. 2016;103:365–76.
[13] Stern ME. The salt-fountain and thermohaline convection. Tellus. 1960;12(2):172–5.
[14] Veronis G. On finite amplitude instability in thermohaline convection. J Mar Res. 1965;23:1–17.
[15] Baines PG, Gill AE. On thermohaline convection with linear gradients. J Fluid Mech. 1969;37(2):289–306.
[16] Shankar BM, Naveen SB, Shivakumara IS. Stability of double-diffusive natural convection in a vertical porous layer. Transp Porous Med. 2022;141:87–105.
[17] Wang L, Chai Z, Shi B. Regularized lattice Boltzmann simulation of double-diffusive convection of power-law nanofluids in rectangular enclosures. Int J Heat Mass Transf. 2016;102:381–95.
[18] Shankar BM, Kumar J, Shivakumara IS. Stability of double-diffusive natural convection in a vertical fluid layer. Phys Fluids. 2021;33(9):094113.
[19] Legare S, Grace A, Stastna M. Double-diffusive instability in a thin vertical channel. Phys Fluids. 2021;33(11):114106.
[20] Bratsun DA, Oschepkov VO, Mosheva EA, Siraev RR. The effect of concentration-dependent diffusion on double-diffusive instability. Phys Fluids. 2022;34(3):034112.
[21] Kerr OS. Double-diffusive instabilities at a vertical sidewall after the sudden onset of heating. J Fluid Mech. 2021;909:A11.
[22] Legare S, Grace A, Stastna M. Double diffusive instability with a constriction. Phys Fluids. 2023;35(2):024109.
[23] Kamotani Y, Wang LW, Ostrach S, Jiang HD. Experimental study of natural convection in shallow enclosures with horizontal temperature and concentration gradients. Int J Heat Mass Transf. 1985;28(1):165–73.
[24] Lee JW, Hyun JM. Double-diffusive convection in a rectangle with opposing horizontal temperature and concentration gradients. Int J Heat Mass Transf. 1990;33(8):1619–32.
[25] Nishimura T, Wakamatsu M, Morega AM. Oscillatory double-diffusive convection in a rectangular enclosure with combined horizontal temperature and concentration gradients. Int J Heat Mass Transf. 1998;41(11):1601–11.
[26] Weaver JA, Viskanta R. Natural convection due to horizontal temperature and concentration gradients—2. Species interdiffusion, Soret and Dufour effects. Int J Heat Mass Transf. 1991;34(12):3121–33.
[27] Qin Q, Xia ZA, Tian ZF. High accuracy numerical investigation of double-diffusive convection in a rectangular enclosure with horizontal temperature and concentration gradients. Int J Heat Mass Transf. 2014;71:405–23.
[28] Ghorayeb K, Mojtabi A. Double diffusive convection in a vertical rectangular cavity. Phys Fluids. 1997;9(8):2339–48.
[29] Makayssi T, Lamsaadi M, Kaddiri M. Natural double-diffusive convection for the Carreau shear-thinning fluid in a square cavity submitted to horizontal temperature and concentration gradients. J Non-Newton Fluid Mech. 2021;297:104649.
[30] Thorpe SA, Hutt PK, Soulsby R. The effect of horizontal gradients on thermohaline convection. J Fluid Mech. 1969;38(2):375–400.
[31] Thangam S, Zebib A, Chen CF. Transition from shear to sideways diffusive instability in a vertical slot. J Fluid Mech. 1981;112:151–60.
[32] Kerr OS, Tang KY. Double-diffusive instabilities in a vertical slot. J Fluid Mech. 1999;392:213–32.
[33] Kerr OS. Oscillatory double-diffusive instabilities in a vertical slot. J Fluid Mech. 2001;426:347–54.
[34] Bahloul A, Mutabazi I, Ambari A. Codimension 2 points in the flow inside a cylindrical annulus with a radial temperature gradient. Eur Phys J Appl Phys. 2000;9(3):253–64.
[35] Zhang JG, Okano Y, Dost S. Effect of radiative heat transfer on thermal-solutal Marangoni convection in a shallow rectangular cavity with mutually perpendicular temperature and concentration gradients. Int J Heat Mass Transf. 2022;183:122104.
[36] Zhang JG, Sekimoto A, Okano Y, Dost S. Numerical simulation of thermal-solutal Marangoni convection in a shallow rectangular cavity with mutually perpendicular temperature and concentration gradients. Phys Fluids. 2020;32(10):102108.
[37] Huang WY, Chen FL. Stability of the double-diffusive convection generated through the interaction of horizontal temperature and concentration gradients in the vertical slot. Phys Fluids. 2023;13(5):055215.
[38] Fourier JBJ. Théorie Analytique de la Chaleur. Paris, France: Firmin Didot; 1822.
[39] Cattaneo C. A form of heat conduction equation which eliminates the paradox of instantaneous propagation. Compt Rend. 1958;247:431–3.
[40] Vernotte P. Some possible complication in the phenomena of thermal conduction. Compt Rend. 1961;252(1):2190–1.
[41] Christov CI. On frame indifferent formulation of the Maxwell–Cattaneo model of finite-speed heat conduction. Mech Res Commun. 2009;36(4):481–6.
[42] Wang MR, Yang N, Guo ZY. Non-Fourier heat conductions in nanomaterials. J Appl Phys. 2011;110(6):064310.
[43] Wang L, Wei X. Heat conduction in nanofluids. Chaos Solitons Fractals. 2009;39(5):2211–5.
[44] Antaki PJ. New interpretation of non-Fourier heat conduction in processed meat. ASME J Heat Transf. 2005;127(2):189–93.
[45] Khayat RE, deBruyn J, Niknami M, Stranges DF, Khorasany RMH. Non-Fourier effects in macro- and micro-scale non-isothermal flow of liquids and gases. Int J Therm Sci. 2015;97:163–77.
[46] Kundu B, Lee KS. Non-Fourier analysis for transmitting heat in fins with internal heat generation. Int J Heat Mass Transf. 2013;64:1153–62.

[47] Abouelregal AE, Ahmad H. Thermodynamic modeling of viscoelastic thin rotating microbeam based on non-Fourier heat conduction. Appl Math Model. 2021;91:973–88.
[48] Dong Y, Cao BY, Guo ZY. Temperature in nonequilibrium states and non-Fourier heat conduction. Phys Rev E. 2013;87(3):032150.
[49] Xu BB, Gao XW, Cui M. High precision simulation and analysis of non-Fourier heat transfer during laser processing. Int J Heat Mass Transf. 2021;178:121574.
[50] Stranges DF, Khayat RE, deBruyn J. Finite thermal convection of non-Fourier fluids. Int J Therm Sci. 2016;104:437–47.
[51] Hughes DW, Proctor MRE, Eltayeb IA. Maxwell-Cattaneo double-diffusive convection: limiting cases. J Fluid Mech. 2021;927:A13.
[52] Bissell JJ. Thermal convection in a magnetized conducting fluid with the Cattaneo-Christov heat flow model. Proc R Soc Lond A. 2016;472(2195):20160649.
[53] Hughes DW, Proctor MRE, Eltayeb IA. Rapidly rotating Maxwell-Cattaneo convection. Phys Rev Fluids. 2022;7(9):093502.
[54] Eltayeb IA. Convective instabilities of Maxwell–Cattaneo fluids. Proc R Soc Lond A. 2016;473(2201):20160712.
[55] Niknami M, Khayat RE. Thermal convection of a non-Fourier fluid in a vertical slot. ASME J Heat Transf. 2016;138(5):052501.
[56] Jakhar A, Kumar A. Instability analysis of double diffusive convection under time dependent solute boundary conditions in the presence of internal heat generator. Phys Fluids. 2023;35(7):077101.

Appendix

A Validity of Squire's theorem

In the case of three-dimensional problems, the basic solutions can be expressed as

$$\begin{aligned}
&\bar{u} = 0, \quad \bar{v} = -\frac{1}{6}\left(1 - \frac{\mathrm{Ra_S}}{\mathrm{GrPr}}\right)x^3 + \frac{1}{24}\left(1 - \frac{\mathrm{Ra_S}}{\mathrm{GrPr}}\right)x,\\
&\bar{w} = 0, \quad \bar{\theta} = x, \quad \bar{S} = x,\\
&\bar{q}_x = -1, \quad \bar{q}_y = \frac{1}{24}C\mathrm{PrGr}\left(1 - \frac{\mathrm{Ra_S}}{\mathrm{GrPr}}\right)(12x^2 - 1),\\
&\bar{q}_z = 0
\end{aligned} \tag{A1}$$

Using infinitesimal disturbances on the fully developed laminar base flow, the solution of the problem can be written in the form

$$\begin{aligned}
&u = \bar{u} + u', \quad v = \bar{v} + v', \quad w = \bar{w} + w',\\
&p = \bar{p} + p', \quad \theta = \bar{\theta} + \theta',\\
&F = \bar{F} + F', \quad S = \bar{S} + S'.
\end{aligned} \tag{A2}$$

Substituting the above expressions of (A2) into Eqs. (11)–(13), (20), and (21), and considering the first order disturbances, the following equations are obtained:

$$\frac{\partial u'}{\partial x} + \frac{\partial v'}{\partial y} + \frac{\partial w'}{\partial z} = 0, \tag{A3}$$

$$\frac{\partial u'}{\partial t} + \mathrm{Gr}\bar{v}\frac{\partial u'}{\partial y} = -\frac{\partial p'}{\partial x} + \left(\frac{\partial^2 u'}{\partial x^2} + \frac{\partial^2 u'}{\partial y^2} + \frac{\partial^2 u'}{\partial z^2}\right), \tag{A4}$$

$$\begin{aligned}
&\frac{\partial v'}{\partial t} + \mathrm{Gr}\left(\frac{\mathrm{d}\bar{v}}{\mathrm{d}x}u' + \bar{v}\frac{\partial v'}{\partial y}\right)\\
&= -\frac{\partial p'}{\partial y} + \left(\frac{\partial^2 v'}{\partial x^2} + \frac{\partial^2 v'}{\partial y^2} + \frac{\partial^2 v'}{\partial z^2}\right) + \theta' - \frac{\mathrm{Ra_S}}{\mathrm{GrPr}}S',
\end{aligned} \tag{A5}$$

$$\frac{\partial w'}{\partial t} + \mathrm{Gr}\bar{v}\frac{\partial w'}{\partial y} = -\frac{\partial p'}{\partial z} + \left(\frac{\partial^2 w'}{\partial x^2} + \frac{\partial^2 w'}{\partial y^2} + \frac{\partial^2 w'}{\partial z^2}\right), \tag{A6}$$

$$\mathrm{Pr}\frac{\partial \theta'}{\partial t} + \mathrm{PrGr}\left(\frac{\mathrm{d}\bar{\theta}}{\mathrm{d}x}u' + \bar{v}\frac{\partial \theta'}{\partial y}\right) = -F', \tag{A7}$$

$$C\mathrm{Pr}\frac{\partial F'}{\partial t} + C\mathrm{PrGr}\bar{v}\frac{\partial F'}{\partial y} = -F' - \frac{\partial^2 \theta'}{\partial x^2} - \frac{\partial^2 \theta'}{\partial y^2} - \frac{\partial^2 \theta'}{\partial z^2}, \tag{A8}$$

$$\begin{aligned}
\frac{1}{\mathrm{Gr}}\frac{\partial S'}{\partial t} + u'\frac{\partial \bar{S}}{\partial x} + \bar{v}\frac{\partial S'}{\partial y} = \frac{1}{\mathrm{GrPrLe}}\Bigg(&\frac{\partial^2 S'}{\partial x^2} + \frac{\partial^2 S'}{\partial y^2}\\
&+ \frac{\partial^2 S'}{\partial z^2}\Bigg).
\end{aligned} \tag{A9}$$

We assume that the perturbation variables take the form

$$\begin{aligned}
&\{u', v', w', p', \theta', S', F'\}\\
&= \{U, V, W, \Pi, \Theta, \Phi, f\}(x)e^{st+i(ay+bz)},
\end{aligned} \tag{A10}$$

where a and b are the real wave numbers in the y and z-directions, respectively, and s dictates the time evolution of the disturbance. Inserting Eq. (A10) in Eqs. (A3)–(A9), we get

$$\frac{\mathrm{d}U}{\mathrm{d}x} + iaV + ibW = 0, \tag{A11}$$

$$(s + ia\bar{v}\mathrm{Gr})U = -\frac{\mathrm{d}\Pi}{\mathrm{d}x} + \frac{\mathrm{d}^2 U}{\mathrm{d}x^2} - (a^2 + b^2)U, \tag{A12}$$

$$\begin{aligned}
&(s + ia\bar{v}\mathrm{Gr})V + \mathrm{Gr}\frac{\mathrm{d}\bar{v}}{\mathrm{d}x}U\\
&= -ia\Pi + \frac{\mathrm{d}^2 V}{\mathrm{d}x^2} - (a^2 + b^2)V + \Theta - \frac{\mathrm{Ra_S}}{\mathrm{GrPr}}\Phi,
\end{aligned} \tag{A13}$$

$$(s + ia\bar{v}\mathrm{Gr})W = -ib\Pi + \frac{\mathrm{d}^2 W}{\mathrm{d}x^2} - (a^2 + b^2)W, \tag{A14}$$

$$s\mathrm{Pr}\Theta + \mathrm{PrGr}\left(\frac{\mathrm{d}\bar{\theta}}{\mathrm{d}x}U + ia\bar{v}\Theta\right) = -f, \tag{A15}$$

$$(sC\mathrm{Pr} + iaC\mathrm{PrGr}\bar{v} + 1)f = -\frac{\mathrm{d}^2\Theta}{\mathrm{d}x^2} + (a^2 + b^2)\Theta, \tag{A16}$$

$$\begin{aligned}
s\frac{1}{\mathrm{Gr}}\Phi + \frac{\partial \bar{S}}{\partial x}U + ia\bar{v}\Phi = \frac{1}{\mathrm{GrPrLe}}\Bigg[&\frac{\mathrm{d}^2\Phi}{\mathrm{d}x^2}\\
&- (a^2 + b^2)\Phi\Bigg].
\end{aligned} \tag{A17}$$

Using the extended Squire's transformation

$$\begin{aligned}
&\tilde{a} = \sqrt{a^2 + b^2}, \quad \tilde{U} = \frac{a}{\tilde{a}}U, \quad \tilde{V} = \frac{a}{\tilde{a}^2}(aV + bW),\\
&\tilde{\bar{v}} = \frac{a}{\tilde{a}}\bar{v}, \quad \tilde{\Pi} = \frac{a}{\tilde{a}}\Pi, \quad \tilde{s} = s, \quad \tilde{\mathrm{Gr}} = \mathrm{Gr},\\
&\tilde{\Theta} = \frac{a^2}{\tilde{a}^2}\Theta, \quad \tilde{\Phi} = \frac{a}{\tilde{a}}\Phi, \quad \tilde{C} = C, \quad \tilde{\bar{\theta}} = \frac{a}{\tilde{a}}\bar{\theta},\\
&\tilde{\mathrm{Ra}}_\mathrm{S} = \frac{a}{\tilde{a}}\mathrm{Ra_S}, \quad \tilde{\mathrm{Pr}} = \mathrm{Pr}, \quad \tilde{\bar{S}} = \bar{S}, \quad \tilde{\mathrm{Le}} = \mathrm{Le},\\
&\tilde{f} = \frac{a^2}{\tilde{a}^2}f.
\end{aligned} \tag{A18}$$

Then, Eqs. (A11)–(A17) become

$$\frac{\mathrm{d}\tilde{U}}{\mathrm{d}x} + i\tilde{a}\tilde{V} = 0, \tag{A19}$$

$$(\tilde{s} + i\tilde{a}\tilde{v}\widetilde{\mathrm{Gr}})\tilde{U} = -\frac{\mathrm{d}\tilde{\Pi}}{\mathrm{d}x} + \frac{\mathrm{d}^2\tilde{U}}{\mathrm{d}x^2} - \tilde{a}^2\tilde{U}, \tag{A20}$$

$$(\tilde{s} + i\tilde{a}\tilde{v}\widetilde{\mathrm{Gr}})\tilde{V} + \widetilde{\mathrm{Gr}}\frac{\mathrm{d}\tilde{v}}{\mathrm{d}x}\tilde{U} = -i\tilde{a}\tilde{\Pi} + \frac{\mathrm{d}^2\tilde{V}}{\mathrm{d}x^2} - \tilde{a}^2\tilde{V} + \tilde{\Theta} - \frac{\widetilde{\mathrm{Ra}}_S}{\widetilde{\mathrm{Pr}}\widetilde{\mathrm{Gr}}}\tilde{\Phi}, \tag{A21}$$

$$\tilde{s}\widetilde{\mathrm{Pr}}\tilde{\Theta} + \widetilde{\mathrm{Pr}}\widetilde{\mathrm{Gr}}\left(\frac{\mathrm{d}\tilde{\theta}}{\mathrm{d}x}\tilde{U} + i\tilde{a}\tilde{v}\tilde{\Theta}\right) = -\tilde{f}, \tag{A22}$$

$$(\tilde{s}\tilde{C}\widetilde{\mathrm{P}}\ \mathrm{r} + i\tilde{a}\tilde{C}\widetilde{\mathrm{Pr}}\widetilde{\mathrm{Gr}}\tilde{v} + 1)\tilde{f} = -\frac{\mathrm{d}^2\tilde{\Theta}}{\mathrm{d}x^2} + \tilde{a}^2\tilde{\Theta}, \tag{A23}$$

$$\tilde{s}\frac{1}{\widetilde{\mathrm{Gr}}}\tilde{\Phi} + \frac{\partial\tilde{\bar{S}}}{\partial x}\tilde{U} + i\tilde{a}\tilde{v}\tilde{\Phi} = \frac{1}{\widetilde{\mathrm{Gr}}\widetilde{\mathrm{Pr}}\widetilde{\mathrm{Le}}}\left(\frac{\mathrm{d}^2\tilde{\Phi}}{\mathrm{d}x^2} - \tilde{a}^2\tilde{\Phi}\right). \tag{A24}$$

The corresponding boundary conditions are

$$\tilde{U} = \tilde{V} = \tilde{\Theta} = \tilde{\Phi} = 0, \quad \text{at} \quad x = \pm\frac{1}{2}. \tag{A25}$$

Eqs. (A19)–(A24) have the same mathematical structure as Eqs. (A11)–(A17) with $w = b = 0$ (*i.e.*, two-dimensional equations). When $b \neq 0$, $\widetilde{\mathrm{Ra}}_S = a/\tilde{a}\mathrm{Ra}_S < \mathrm{Ra}_S$. Therefore, the solute Rayleigh number at which modal instability occurs for two-dimensional infinitesimal disturbances is lower than that for three-dimensional infinitesimal disturbances. Hence, it suffices to investigate the modal instability of double-diffusive convection in a vertical fluid layer using two-dimensional disturbances.